ChemComm

Accepted Manuscript

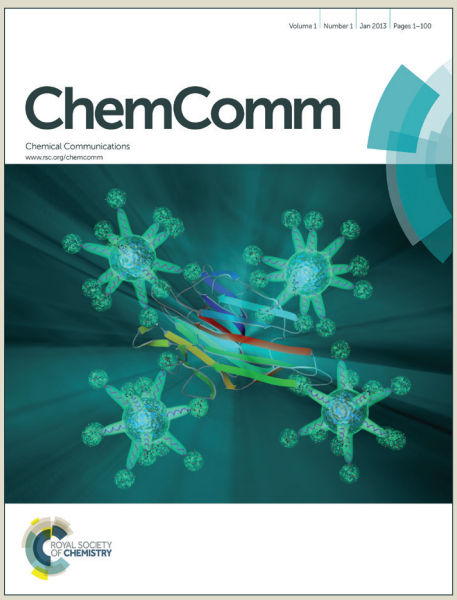

ROYAL SOCIETY OF CHEMISTRY

www.rsc.org/chemcomm

Journal Name

RSCPublishing

COMMUNICATION

The Crystallinity Effect of Mesocrystalline $BaZrO_3$ Hollow Nanospheres on Charge Separation for Photocatalysis

Tian-Nan Ye,[a] Miao Xu,[a] Wei Fu,[a] Yi-Yu Cai,[a] Xiao Wei,[a] Kai-Xue Wang,[a] Yong-Nan Zhao,[b] Xin-Hao Li*[a] and Jie-Sheng Chen*[a]

Cite this: DOI: 10.1039/x0xx00000x

Received 00th January 2012,
Accepted 00th January 2012

DOI: 10.1039/x0xx00000x

www.rsc.org/

Highly crystalline $BaZrO_3$ mesocrystal hollow nanospheres offered higher photocatalytic activities. It is found that the high crystalline sample can function as "highway" for electron transport with less grain boundaries, resulting in better charge separation and thus photocatalytic performance.

Enhancing the activity of photocatalysts for artificial photosynthesis and environmental purification mainly lies in the capability of absorbing light and the quantum yield.[1-3] The quantum yield of photocatalyst is dictated by the ability to suppress the fast combination of photogenerated electrons and holes as well as to transfer the as-formed charge carriers to the active sites.[4-5] For inorganic photocatalysts, such as metal oxides and metal nitrides, their crystal form dominates the process of charge separation and transfer for photocatalysis to a great extent.[6-7] Recent efforts to study the effect of crystal form on the activity of photocatalysts were mainly focused on crystal-facet effect of various nano-photocatalyst.[8-10] It is believed that high crystallinity of inorganic photocatalysts can be beneficial for charge separation and transfer, promising access to the improved photocatalytic activity.[11] Highly crystalline nanostructure can function as "highway" for electron transport with less grain boundaries.

Recently, mesocrystals of various semiconductive materials have received rapidly much attention due to their promising applications including photocatalysis, solar cells, and energy storage.[12-16] Mesocrystals are characterized by their high porosity, ordered subunit alignment, and thus relatively less defects among grain boundary as compared with disordered assemblies of nanoparticles.[17] Consequently, mesocrystal-based photocatalysts was thus believed to offer better photo-harvesting efficiency as compared with that of irregular aggregates. In principle, a certain amount of defects among grain boundary can act as trapping and recombination centers between photogenerated electrons and holes, resulting in a decrease in the photocatalytic activity.[18-19] Elevating the crystallinity is a possible measure to overcome this drawback. Studies on the direct correlation between mesocrystals crystallinity (or amounts of defects) and the photocatalytic performance are of great significance for the design of novel and highly efficient photocatalysts. However, the success in engineering the crystallinity of semiconductor mesocrystals is rare.

In order to study the crystallinity effect of mesocrystals on the final photocatalytic activity, fabrication of mesocrystal line nanocatalysts with gradually increased crystallinity is necessary but challenging. Calcinating semiconductor materials at elevated temperature should be the most direct pathway to gradually improve their crystallinity. Unfortunately, aggregation is usually inevitable, resulting in an obvious decrease in the surface area. The benchmark semiconductor material TiO_2, is an excellent choice for photocatalytic H_2 production; however, the poor stability of their crystal structure, nanostructure and/or composition at high temperatures will inflict severe limitations on directly demonstrating the effect of crystallinity on their photocatalytic activity.[20] $BaZrO_3$, a typical cubic perovskite oxide, is a promising material applied in high-temperature microwave dielectrics with excellent thermal stability.[21] Recently, Zou et al. reported the photocatalytic activity of both the bare and doped $BaZrO_3$ powders for water splitting.[22-23] It is worth noting that the crystal structure of $BaZrO_3$ could remain stable at a temperature up to 1000 °C; meanwhile the aggregation of small nanoparticles with much lowered surface area is inevitable after a calcination at very high temperature. More importantly, the crystallinity of $BaZrO_3$ materials could be gradually enhanced through a simple calcination process at gradually elevated temperature. A perfect model for investigating the crystallinity effect of mesocrystal for photocatalytic activity should have gradually changed crystallinity with similar morphology and surface areas. Considering that low-dimensional nanostructures tend to aggregate after calcination at high temperature, we thus choose $BaZrO_3$ hollow nanospheres in this work due to their stable mesostructure with fixed thickness of the shell in nanoscale. The photocatalytic activity of highly crystalline $BaZrO_3$ hollow nanospheres is nearly two times of that of the

meso-crystalline hollow nanospheres with relatively lower crystallinity and five times higher than that of disordered bulk crystals.

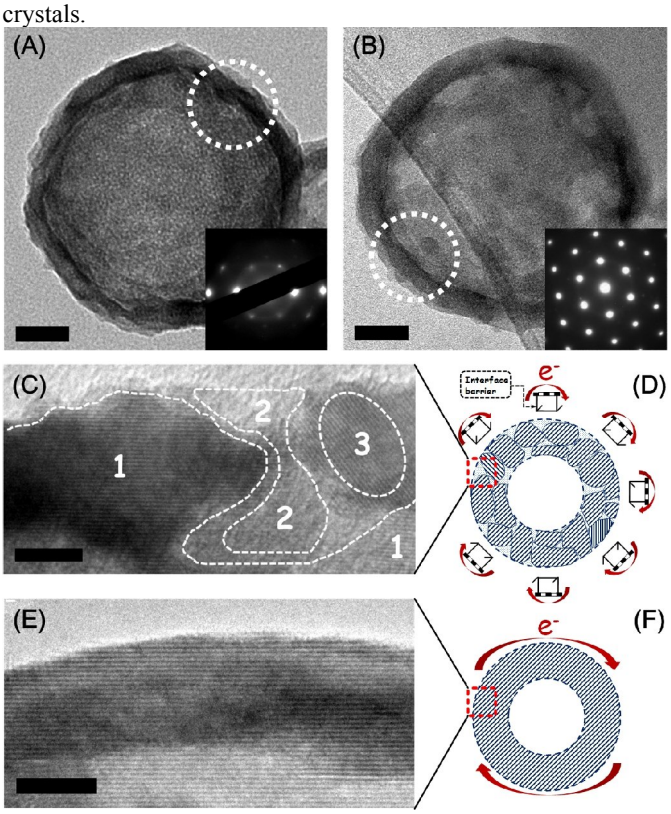

Fig. 1 Typical TEM images of individual hollow nanospheres (A) BZO-mc and (B) BZO-1000. Insets (A, B): corresponding SAED patterns of the white dotted cycles; (A, B) scale bar: 20 nm. HRTEM images and corresponding schematic models of the shells (C, D) BZO-mc and (E, F) BZO-1000. In (D, F) the e^- and red arrows represent the photocatalysis process of the photogenerate electrons that transferred around the outer surface of the hollow nanospheres. Inset (C): area 1 host lattice, area 2 and 3 disordered domain. Inset (D): the "hurdles frames" represents the interface barrier among the outer surface grain boundaries. (C, E) Scale bar: 5 nm.

$BaZrO_3$ hollow nanospheres were prepared by a modified hydrothermal method (Fig. 1 and Fig. S1, ESI†). The as-obtained sample was composed of small nanocrystals assembled via oriented attachment (Fig. 1C and Fig. S2A, ESI†), in another word, mesocrystal hollow nanospheres, and was thus denoted as BZO-mc. When the as-formed sample BZO-mc was calcined at elevated temperature from 600 °C via 800 °C to 1000 °C, the crystalline phase (perovskite phase) and composition (Fig. S3, ESI†) of the post-treated $BaZrO_3$ samples (BZO-600, BZO-800 and BZO-1000) remained the same without the formation of other phase of $BaZrO_3$ as revealed by the XRD patterns (Fig. 2A, S4, ESI†). Higher calcination temperature was also invesgated in Fig. S5 (ESI†). The hollow structures and sizes (Fig. S6, ESI†) of these post-treated $BaZrO_3$ hollow nanospheres were preserved well (Fig. 1B) with a fixed thickness of the shells (Fig. 1E and Fig. S7, ESI†) and slightly decreased surface areas (Fig. S8, ESI†). More importantly, the crystallinity of the $BaZrO_3$ mesocrystal hollow nanospheres increased linearly with the elevated calcination temperature as demonstrated by the gradually sharpened diffraction peaks. As shown in the XRD patterns (Fig. 2B and Fig. S4, ESI†), the (110) peak of BZO-1000 became much stronger and narrower with a full width at half-maximum (FWHM) of only 0.181°, which is much lower than that of BZO-mc (0.454°). Such a trend was general for all the XRD peaks (Fig. 2B) of those samples, revealing the gradually enhanced crystallinity.

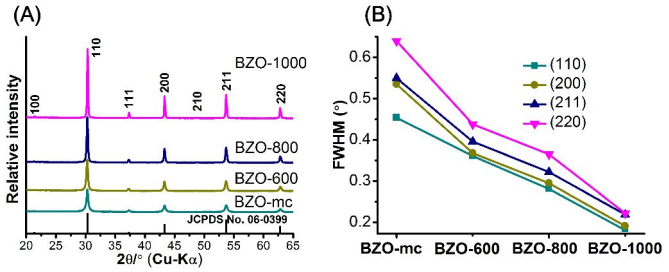

Fig. 2 (A) XRD patterns, (B) Full widths at half-maximum (FWHM) of the typical BZO-mc, BZO-600, BZO-800 and BZO-1000 XRD peaks.

Given that the crystallinity of the $BaZrO_3$ mesocrystal hollow nanospheres were successfully tuned without changing their morphology and composition, we are interested in studying the crystallinity-dependent photocatalytic activity of these samples. We initially tested the availability of $BaZrO_3$ samples for reducing water to release H_2 gas. Steady H_2 production from water containing different sacrificial electron donors (Table S1, ESI†) can be achieved over $BaZrO_3$ samples. Noble metal cocatalyst is not required. The H_2 production rate increases with the increased crystallinity of the $BaZrO_3$ samples. The BZO-1000 offered the highest activity for H_2 production and possessed excellent sustainablity (Fig. S9, S10, ESI†). After excluding the effect of surface area on the photocatalytic activity of the $BaZrO_3$ mesocrystal hollow nanospheres (Fig. 3A), the promotion effect of the highly crystalline nanostructures is much better seen by the significant increase in the normalized H_2 evolution rates (Table S2, ESI†). Additionly, the constant XRD peak ratio of (110)/(111) for the four samples also excluded the effect of specific crystals facets on the photocatalytic activity (Table S3, ESI†).

In order to investigate the intrinsic effect of the crystallinity on the photocatalytic performance of $BaZrO_3$ mesocrystal hollow nanospheres, further investigations on its composition, structure and properties were conducted. The band gaps of $BaZrO_3$ samples calcined at different temperatures are all estimated to be 4.8 eV from the UV-diffuse absorption spectrum (Fig. S11, ESI†). This result excludes the possible effect of the varied band structure on the enhanced photocatalytic activity of the post-treated $BaZrO_3$ samples.

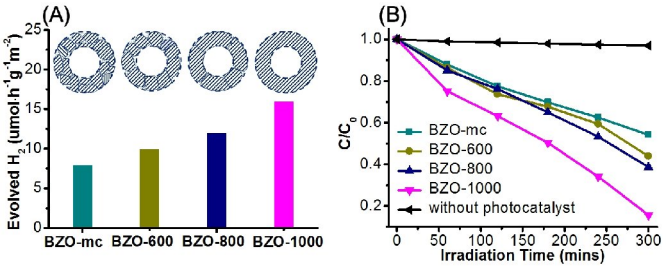

Fig. 3 (A) Typical surface-specific photocatalytic activities of H_2 production, and (B) MO degradation efficiency curves of the BZO-mc, BZO-600, BZO-800 and BZO-1000 respectively.

HRTEM images reveal the real structure of the surface of these samples. As a typical sample with low crystallinity, the as-obtain BZO-mc is far from ideal crystals with disordered domains (area 2 and 3 in Fig. 1C and Fig. S2A, ESI†). After a calcination at 1000 °C the shell of BZO-1000 turns to well

crystalline nature according to the regular and oriented lattice fringed shown in Fig. 1E and Fig. S2B (ESI†). Amorphous areas or disordered domains were rarely observed in BZO-1000. Meanwhile, the SAED pattern became more clearly (Fig. 1), which indicated that the primary nanoparticles grow larger with the constant shell thickness after calcinations (Fig. S7, ESI†).

All the results mentioned above suggested that most of the defects on the surface or interface of these primary nanoparticles were removed after calcination. This can be further confirmed by the XPS analysis (Fig. S12, ESI†). The peak at 529.1 eV is associated with the oxygen atoms in the lattice and the peak with a higher binding energy 531.1 eV is associated with the O^{2-} ions in the oxygen-deficient regions within the matrix of $BaZrO_3$.[24-26] The gradually weakened binding energy peaks at 531.1 eV of the post-treated $BaZrO_3$ hollow nanospheres reveals less oxygen-deficient regions, which are mainly grain boundary defects in these samples. This is presumably due to the increase in the crystallinity of those samples, which has already been demonstrated by the XRD and HRTEM analysis.

Further analysis on the pore size distributions of these samples were also conducted (Fig. S13, ESI†). It is obvious that these pores within the range of 3-7 nm could only be attributed to the voids between the primary nanocrystals, whilst the aggregation pores between the secondary hollow spheres (mean size > 70 nm) should be larger. As a result, the decrease in inter-particle voids between primary particles and thus less grain boundaries could be somewhat reflected by the pore size distribution at the range of several nanometers.

Less grain boundary defects, and well developed crystal structures means less traps for charge carriers (Fig. 1F) to move to the active sites on the surface. All these merits are beneficial for enhancing the effective charge transfer with less electron-hole recombination. As expected, there is a considerable decrease in the fluorescent intensity (Fig. S14, ESI†) and sub-bandgap absorption (Fig. S11, ESI†) of the post-treated samples. Moreover, the mashed nanostructure will not obviously affect the fluorescent intensity and photocatalytic activity of our hollow nanospheres (Fig. S15, ESI†). Therefore, the crystallinity-dependent fluorescent intensity directly reveals the much lower recombination probability of photo-generated electrons and holes in the highly crystalline $BaZrO_3$ samples. In principle, the low recombination rate of electrons and holes is often associated with highly photocatalytic activity, not limited to the electron-consuming H_2 evolution reaction via water splitting. We thus further tested the oxidation strength of all the samples by choosing photocatalytic decomposition of methyl orange (MO) as a model reaction. Indeed, the degradation rate of MO also increases with the increased crystallinity of the $BaZrO_3$ samples (Fig. 3B). Consequently, high crystallinity of photocatalysts is a general factor that can enhance the photocatalytic activity by promoting the charge separation.

In summary, we demonstrated the direct evidence of the crystallinity effect of mesocrystal on the photo-conversion efficiencies by using $BaZrO_3$ hollow nanosphere as an ideal photocatalyst model here. The lower recombination of the electrons and holes in the highly crystalline photocatalysts are beneficial for improving their photocatalytic activities, including high activity for hydrogen production from water splitting and MO degradation. This work provides us a better understanding on the real effect of the crystallinity on the photocatalytic performance of mesocrystal photocatalysts. More importantly, high crystallinity should be the key factor to be considered besides band structure and morphology in preparing and designing novel photocatalysts in nanoscale.

This work was supported by the National Basic Research Program of China (2013CB934102, 2011CB808703) and the National Natural Science Foundation of China.

Notes and references

[a]School of Chemistry and Chemical Engineering, Shanghai Jiao Tong University, Shanghai 200240, P. R. China.
E-mail: xinhaoli@sjtu.edu.cn; chemcj@sjtu.edu.cn.
[b]Institute of Nanostructured Materials & Tianjin Key Laboratory of Fiber Modification and Functional Fiber, School of Materials Science and Engineering, Tianjin Polytechnic University, Tianjin 300387, P. R. China.

†Electronic Supplementary Information (ESI) available. See DOI:10.1039/c000000x/

1 K. Maeda, K. Teramura, D. Lu, T. Takata, N. Saito, Y. Inoue and K. Domen, *Nature*, 2006, **440**, 295.
2 Z. G. Zou, J. H. Ye, K. Sayama and H. Arakawa, *Nature*, 2001, **414**, 625.
3 A. Kudo and Y. Miseki, *Chem. Soc. Rev.*, 2009, **38**, 253.
4 X. Chen, S. Shen, L. Guo and S. Mao, *Chem. Rev.*, 2010, **110**, 6503.
5 K. Maeda and K. Domen, *J. Phys. Chem. Lett.*,2010, **1**, 2655.
6 J. Zhang, X. Qian, Z. C. Feng, M. J. Li and C. Li, *Angew. Chem. Int. Ed.*, 2008, **47**, 1766.
7 J. Zhang, M. J. Li, Z. C. Feng, J. Chen and C. Li, *J. Phys. Chem. B*, 2006, **110**, 927.
8 J. Pan, G. Liu, G. Q. Lu and H. M. Cheng, *Angew. Chem. Int. Ed.*, 2011, **50**, 2133.
9 G. Liu, J. C.Yu, G. Q. Lu and H. M. Cheng, *Chem. Commun.*, 2011, **47**, 6763.
10 J. Pan, X. Wu, L. Z. Wang, G. Liu, G. Q. Lu and H. M. Cheng, *Chem. Commun.*, 2011, **47**, 8361.
11 X. H. Li, J. S. Zhang, X. F. Chen, A. Fischer, A. Thomas, M. Antonietti and X. C. Wang, *Chem. Mater.*, 2011, **23**, 4344.
12 J. F. Ye, L. Wen, J. G. Cai, S. Chen, X. W. Zhao, H. H. Zhou and L. M. Qi, *J. Am. Chem. Soc.*, 2011, **133**, 933.
13 R. Q. Song and H. Cölfen, *Adv. Mater.*, 2010, **22**, 1301.
14 W. H. Lin, T. F. M. Chang, Y. H. Lu, T. Sato, M. Sone, K. H. Wei and Y. J. Hsu, *J. Phys. Chem. C*, 2013, **117**, 25596.
15 W. Jiao, L. Z. Wang, G. Liu, G. Q. Lu and H. M. Cheng, *ACS Catal.*, 2012, **2**, 1854.
16 M. S. Wang, Y. P. Zhang, Y. J. Zhou, F. W. Yang, E. J. Kim, S. H. Hahn and S. G. Seong, *CrystEngComm.*, 2013, **15**, 754.
17 H. Cölfen and M. Antonietti, *Angew. Chem. Int. Ed.*, 2005, **44**, 5576.
18 P. Tartaj, *Chem. Commun.*, 2011, **47**, 256.
19 P. Tartaj and J. M. Amarilla, *Adv. Mater.*, 2011, **23**, 4904.
20 G. Liu, J. Pan, L. C. Yin, J. T. S. Irvine, F. Li, J. Tan, P. Wormald and H. M. Cheng, *Adv. Funct. Mater.*, 2012, **22**, 3233.
21 G. Lupina, O. Seifarth, G. Kozlowski, P. Dudek, J. Dabrowski, G. Lippert and H. J. Müssig, *Microelectron. Eng.*, 2009, **86**, 1842.
22 Y. P. Yuan, X. L. Zhang, L. F. Liu, X. J. Jiang, J. Lv, Z. S. Li and Z. G. Zou, *Int. J. Hydrogen. Energ.*, 2008, **33**, 5941
23 Y. P. Yuan, Z. Y. Zhao, J. Zheng, M. Yang, L. G. Qiu, Z. S. Li and Z. G. Zou, *J. Mater. Chem.*, 2010, **20**, 6772.
24 W. P. Sun, M. F. Liu and W. Liu, *Adv. Energy Mater.*, 2013, **3**. 1041.
25 Y. D. Zhu, M. Y. Li, H. Zhou, Z. Q. Hu, X. L. Liu, X. L. Fang, B. Sebo, G. J. Fang and X. Z. Zhao, *J. Phys. D: Appl. Phys.*, 2012, **45**, 375303.
26 A. Younis, D. Chu and S. Li, *J. Phys. D: Appl. Phys.*, 2012, **45**, 355101.